# Immobilization of Co−Al Layered Double Hydroxides on Graphene Oxide Nanosheets: Growth Mechanism and Supercapacitor Studies

Shu Huang,[†] Guan-Nan Zhu,[‡] Chao Zhang,[†] Weng Weei Tjiu,[§] Yong-Yao Xia,[‡] and Tianxi Liu*,[†]

[†]State Key Laboratory of Molecular Engineering of Polymers, Department of Macromolecular Science, and [‡]Department of Chemistry and Shanghai Key Laboratory of Molecular Catalysis and Innovative Materials, Institute of New Energy, Fudan University, Shanghai 200433, P. R. China

[§]Institute of Materials Research and Engineering, A*STAR (Agency for Science, Technology and Research), 3 Research Link, Singapore 117602, Singapore

ⓢ *Supporting Information*

**ABSTRACT:** Layered double hydroxides (LDHs) are generally expressed as $[M^{2+}_{1-x}M^{3+}_x(OH)_2][A^{n-}_{x/n}\cdot mH_2O]$, where $M^{2+}$ and $M^{3+}$ are divalent and trivalent metal cations respectively, and A is $n$-valent interlayer guest anion. Co−Al layered double hydroxides (LDHs) with different sizes have been grown on graphene oxide (GO) via in situ hydrothermal crystallization. In the synthesis procedure, the GO is partially reduced in company with the formation of Co−Al LDHs. The morphology and structure of LDHs/GO hybrids are characterized by transmission electron microscopy (TEM), scanning electron microscopy (SEM), X-ray diffraction (XRD), X-ray photoelectron spectroscopy (XPS) and Raman spectroscopy. The growth mechanism of LDHs on GO



Growing LDH on graphene oxide film

20 μm
Graphene oxide film

At high ion concentration

10 μm
LDHs orientated with ab-faces perpendicular to the substrate

nanosheets is discussed. Moreover, both LDHs and LDHs/graphene nanosheets (GNS) hybrids are further used as electrochemical supercapacitor materials and their performance is evaluated by cyclic voltammetry (CV) and galvanostatic charge/discharge measurements. It is shown that the specific capacitances of LDHs are significantly enhanced by the hybridization with GNS.

**KEYWORDS:** *layered double hydroxide, graphene oxide, hybrids, growth mechanism, supercapacitor*
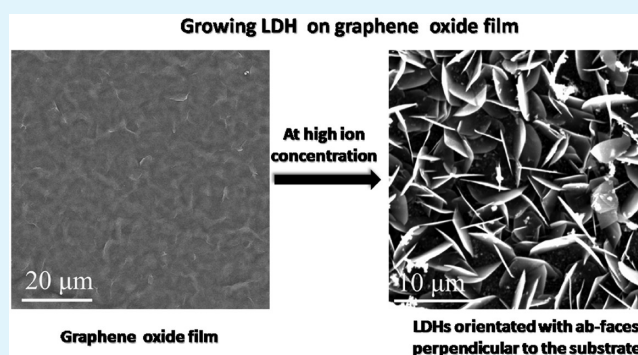
## 1. INTRODUCTION

Layered double hydroxides (LDHs), also known as anionic or hydrotalcite-like clays, are generally expressed as $[M^{2+}_{1-x}M^{3+}_x(OH)_2][A^{n-}_{x/n}\cdot mH_2O]$, where $M^{2+}$ and $M^{3+}$ are divalent and trivalent metal cations respectively, and A is $n$-valent interlayer guest anion. The positive charge of the layer is generated by the replacement of a portion of divalent metal cation of brucite-like layer with a trivalent cation and is compensated for by the interlayer anions. LDHs have been widely studied in fields of catalysts,[1,2] storage and triggered release of functional anions,[3,4] optical materials,[5,6] flame retardants,[7] and nanofillers.[8] Recently, the growth of LDHs on various substrates has received considerable attention.[9] For example, Zn−Al LDHs film and Cu−Al LDHs film were grown on Zn and Cu foil, respectively, by suspended a Zn (or Cu) foil and a Al foil into an alkaline solution ($Na_2CO_3$ + $NH_3\cdot H_2O$) at room temperature.[10] Mg−Al LDHs films with different orientations on the two sides of a glass substrate, one of which was modified with poly(vinyl alcohol), have been obtained by a one-step in situ hydrothermal crystallization method.[11] Highly oriented Li−Al LDHs films were grown on substrates such as glass, Si wafer and carbon cloth in an aqueous alkaline $Al^{3+}$- and $Li^+$-containing solution.[12] However, most of

the substrates used act as metal ion sources or simple supports, which cannot endow new functions to LDHs. Therefore, finding suitable materials, which can simultaneously support and form complexes or hybrids with LDHs as well as be able to endow LDHs with additional performance, has become new challenges for the growth of LDHs on various substrates.

Graphene, as a one-atom-thick graphitic carbon material, has received enormous interests owing to its large specific surface area, excellent electrical and thermal conductivities and high stiffness.[13] Unfortunately, the graphene sheets obtained by direct reduction of graphene oxide (GO) sheets in water usually result in irreversibly agglomerated structure due to the increase in hydrophobic and π-stacking interactions of recovered graphite domains of reduced graphene oxide (RGO) sheets.[14] The prevention of aggregation is essential for graphene nanosheets because most of their unique properties are only associated with individual sheets. Hybridizing graphene with LDHs is an effective way to solve this problem. The decorating LDHs can decrease the restacking

interactions and aggregation of graphene nanosheets (GNS). In addition, the large specific surface area GNS which act as a substrate can endow LDHs new properties such as electrical and thermal conductivities.

The types of $M^{n+}$ and $A^{n-}$ vary over a wide range, giving rise to a large class of LDHs materials. LDHs materials containing transition metals (such as Co–Al, Fe–Al, and Ni–Al) have been reported to be promising electrode materials for supercapacitors because of their relatively low fabrication cost and high redox activity.[15] To present, several kinds of transition metals LDHs/graphene hybrids were prepared by in situ crystallization in the presence of GO dispersion. Li et al. fabricated Ni–Fe LDHs/RGO hybrid by the hydrothermal treatment of a mixed suspension of the exfoliated graphite oxide.[16] Gao et al. prepared Ni–Al LDHs/RGO hybrid by a hydrothermal method for supercapacitor material.[17] They all considered that the LDHs grow on the surface of GO, but the growth mechanism of LDHs on GO has not been explored.

In this work, microsized and nanosized Co–Al LDHs, for the first time, in situ grew on GO, respectively. The introduction of Co–Al LDHs on the surface of GO nanosheet impedes GO to restore the graphite structure during hydrothermal reduction process. After comparative study of the morphology of Co–Al LDHs grown on individual GO nanosheets and vacuum-filtered graphene oxide film, we proposed a model to describe the growth process of LDHs on GO. Furthermore, Co–Al LDHs and Co–Al LDHs/GNS hybrids as electrochemical supercapacitors materials were studied.

## 2. EXPERIMENTAL SECTION

**2.1. Reagents and Materials.** $CoCl_2 \cdot 6H_2O$, $AlCl_3 \cdot 6H_2O$, NaOH, $N_2H_4 \cdot H_2O$, $NH_3 \cdot H_2O$, $Na_2CO_3$, and urea were supplied by China Medicine Co. Natural graphite powder (325 mesh) was commercially obtained from Alfa-Aesar. All reactants were of analytical purity and used as received. Ultrapure Milli-Q water was used throughout all the experiments.

**2.2. Synthesis of Nanosized and Microsized Co–Al–CO$_3$ LDHs.** Microsized Co–Al LDHs were synthesized according to our previous report.[18] $CoCl_2 \cdot 6H_2O$, $AlCl_3 \cdot 6H_2O$, and urea were dissolved in 100 mL deionized water to give the final concentrations of 10, 5, and 35 mM, respectively. The aqueous mixture was allowed to react in a 100 mL Teflon-lined autoclave at 100 °C for 24 h. After cooling to room temperature, the solid products were filtered, subsequently washed with deionized water and anhydrous ethanol for several times, and finally air-dried at room temperature.

Nanosized Co–Al LDHs were prepared by a fast nucleation and a subsequent hydrothermal treatment.[19,20] Typically, 10 mL of $CoCl_2$ (2.0 mmol) and $AlCl_3$ (1.0 mmol) solution was quickly added (within 5 s) into 40 mL of NaOH (6 mmol) and $Na_2CO_3$ (0.52 mmol) solution under vigorous stirring, followed by stirring for another 20 min. The LDHs nuclei were obtained via centrifugation and washed twice with deionized water. After that, the LDHs nuclei were dispersed in 40 mL of deionized water and reacted in a 100 mL Teflon-lined autoclave at 100 °C for 24 h. After air-cooling, a pink and stable LDHs suspension was obtained. LDHs were collected with high-speed centrifugation (13 000 rpm), subsequently washed with deionized water and anhydrous ethanol for several times, and finally air-dried at room temperature.

**2.3. Synthesis of LDHs/GO Hybrid and LDHs/GNS Hybrid.** Graphite oxide was prepared using a modified Hummers' method from graphite powder.[21] GO suspension (1 mg/mL) was achieved by ultrasonicated exfoliation of 100 mg graphite oxide in 100 mL water for 1 h. The microsized Co–Al LDHs/GO hybrid was synthesized via an in situ crystallization technique. Briefly, $CoCl_2 \cdot 6H_2O$, $AlCl_3 \cdot 6H_2O$, and urea were dissolved in 20 mL deionized water to give the final concentrations of 5, 10, and 35 mM. The mixture was added into 20

mL GO suspension above prepared. After being sonicated for 30 min, the suspension reacted in a 100 mL Teflon-lined autoclave at 100 °C for 24 h. The resulting black product was filtered and washed with deionized water, then dried in air. The nanosized Co–Al LDHs/GO hybrid was synthesized by hydrothermal treatment of LDHs nuclei/ graphene oxide suspension. First, the LDHs nuclei suspension (40 mL) is formed by the same method of preparing nanosized Co–Al LDHs. Eight mL nuclei suspension was then taken out and added into 40 mL of graphene oxide suspension. After vigorously stirred for 30 min, the aqueous suspension was allowed to react in a 100 mL Teflon-lined autoclave at 100 °C for 24 h. After being cooled to room temperature, the solid products were filtered, subsequently washed with deionized water for several times, and finally air-dried at room temperature.

LDHs/GNS hybrid was prepared by reduction of LDHs/GO hybrid with hydrazine hydrate. In a typical procedure, LDHs/GO hybrid (100 mg) was loaded in a 250-mL round-bottom flask and water (100 mL) was then added, was then reduced with 60 $\mu$L of 50 wt % hydrazine hydrate at 95 °C for 2 h to obtain LDHs/GNS hybrid.

**2.4. Characterization.** Transmission electron microscopy (TEM) observations were performed under an acceleration voltage of 200 kV with a Philips CM 300 FEG TEM. Scanning electron microscope (SEM, Tescan 5136 MM) was also used to observe the samples. The samples were coated with gold prior to observation. Atomic force microscopy (AFM) images were acquired in tapping mode by using a Nanoscope IV from Digital Instruments. For AFM observations, the samples were prepared by casting and drying the solution on freshly cleaved mica at room temperature. The Co and Al contents of the LDHs and LDHs/GNS samples were measured by inductively coupled plasma (ICP) atomic emission spectroscopy (Hitachi P-4010) after dissolving a weighed amount of sample with an aqueous HCl solution. X-ray diffraction (XRD) patterns of the samples were conducted on an X'Pro X-ray diffractometer with Cu K$\alpha$ radiation ($\lambda$ = 0.1548 nm) under a voltage of 40 kV and a current of 40 mA. Fourier transform infrared spectroscopy (FTIR) were recorded with a 4 cm$^{-1}$ spectral resolution on a Nicolet Nexus 470 spectrometer equipped with a DTGS detector by signal averaging 64 scans. IR samples were in the form of KBr pellets containing 2 wt % predried sample material.

Electrochemical characterization was carried out as follows: The as-prepared LDHs or LDHs/GNS hybrid, acetylene black, and poly(tetrafluoroethylene) (PTFE) were mixed in a mass ratio of 80:15:5 and dispersed in ethanol to produce a homogeneous paste. Then the resulting mixture was pressed onto a piece of foamed Ni grid under a pressure of 20 MPa. Finally, the fabricated electrode was dried at 80 °C for 8 h in a vacuum oven. All the electrochemical measurements were performed under a three-electrode cell at room temperature: the Ni foam coated with LDHs/GNS hybrid was used as the working electrode, and a Pt foil (1 cm$^2$) and a saturated calomel electrode (SCE) were used as the counter and reference electrodes, respectively; 1 M KOH aqueous solution was prepared as the electrolyte. Cyclic voltammetry (CV) tests and galvanostatic charge/ discharge curves were carried out by a CHI-605B type electrochemical workstation.

## 3. RESULTS AND DISCUSSION

**3.1. Structure and Morphology of LDHs and GO.** Formation of LDHs crystallites involves two stages: nucleation and growth, which will influence the crystallite size and crystallite size distribution.[22] LDHs have their own advantages in terms of purity, control of crystallinity and particle size, wider possibility of functionalization, and composition of chemical elements.[23] Microsized LDHs samples are prepared by precipitation through urea hydrolysis approach under hydrothermal condition. During the heating process, urea hydrolyzes to raise pH homogeneously in solution, which often results in a slow nucleation. Figure 1 shows a TEM image of a typical microsized Co–Al LDHs sample. The sample consists of hexagonal platelets with a lateral size as large as about 5 $\mu$m,
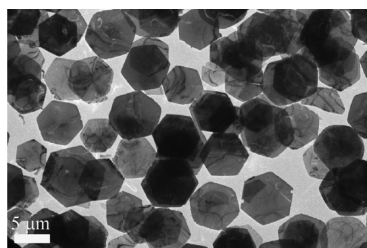
**Figure 1.** TEM image of microsized Co−Al LDHs.

which is of high quality in terms of size, uniformity, and crystallinity. In contrast, nanosized LDHs were synthesized by a very fast nucleation method. The LDHs nuclei are formed in a short time with the addition of high concentration NaOH solution, and then these nuclei grow in the solution for 24 h.[23] Figure 2a shows a TEM image of a typical nanosized Co−Al
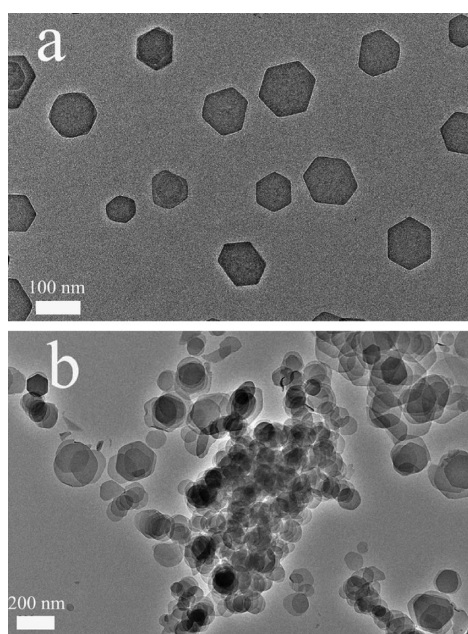


**Figure 2.** TEM images of nanosized Co−Al LDHs: (a) before and (b) after vacuum drying.

LDHs sample. The LDH sample was thin hexagonal platelets with a lateral size in the range of 40−60 nm. However, because of the high surface energy and strong van der Waals interactions, it is hard for vacuum-dried nanosized Co−Al LDHs to redisperse in water. Aggregated LDHs were observed even after ultrasonication for 20 min in water, as shown in Figure 2b. However, vacuum-drying-induced agglomeration is not observed for microsized LDHs, indicating week particle−particle interaction.

XRD is a powerful and essential apparatus for evaluating the structure of LDHs. As shown in Figure 3, both microsized LDHs and nanosized LDHs exhibited the characteristic LDHs structure. The strong peaks at $2\theta = 11.8°$ and $23.7°$ correspond to (003) and (006) diffraction planes of LDHs, respectively. According to the Bragg equation, the basal distance was calculated to be 0.8 nm, indicating the presence of $CO_3^{2-}$ in the interlayer. Compared with nanosized LDHs, the microsized LDHs show a much stronger (003) diffraction peak, demonstrating a higher crystallinity. In addition, ICP and FTIR were used to study the composition of the as-prepared
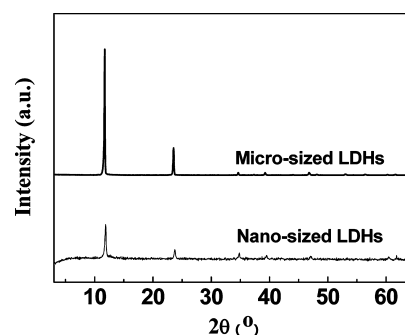


**Figure 3.** XRD curves of microsized LDHs and nanosized LDHs.

Co−Al LDHs. The molar ratio of Co/Al is determined to be 1.94 by elemental analysis using ICP-AES analysis. FTIR spectra of the as-prepared Co−Al LDHs sample are shown in Figure S1 in the Supporting Information. The strong peaks at 1356 cm$^{-1}$ and 790 cm$^{-1}$ correspond to the $\nu3$ vibration and bending modes of $CO_3^{2-}$, respectively. The weak peak at 1607 cm$^{-1}$ is due to the bending mode of water molecules. Other absorption bands below 800 cm$^{-1}$ are associated with metal−oxygen (M−O) stretching and bending modes. Therefore, XRD results and FTIR spectra confirm that microsized and nanosized Co−Al−$CO_3$ LDHs samples have been successfully synthesized.

GO, acting as the substrate for the growth of LDHs, is examined by TEM and AFM. See Figure S2 in the Supporting Information shows the TEM image at low magnification for the GO sheets which tend to congregate together to form wrinkled or multilayer agglomerates. Some individual nanosheets can also be observed, having dimensions of several hundred to several thousand nanometers. Tapping-mode AFM image of GO (see Figure S3 in the Supporting Information) shows two-dimensional, irregular ultrathin sheets with lateral dimensions of up to about 0.5 $\mu$m. The height profile in Figure S3 in the Supporting Information reveals that the nanosheets have an average thickness of about 0.9 nm. This value indicates that a successful exfoliation and unilamellar GO sheets have been obtained.[24]

**3.2. Structure, Morphology, and Growth Mechanism of LDHs/GO Hybrids.** GO has been demonstrated as an ideal single-atom thick substrate for the growth of functional nanomaterials. Oxygen-containing defect sites on GO can absorb positive anion or nanoparticle and offer nucleation site for the growing of nanoparticles. Different from growing sphere-shaped particles on the GO surface, the anisotropy is very important consideration for LDHs in both theory and practice. It is anticipated that LDHs could exhibit two distinct orientations: LDHs with the *ab* face of the crystallites perpendicular or parallel to the substrate.

Figure 4 shows the TEM images of microsized LDHs/GO hybrid. Both microsized LDHs and GO nanosheets are clearly observed, as indicated by the white arrows and black arrows, respectively. LDHs sample kept hexagonal shape but with different orientations on the graphene surface. Some LDHs grow with *ab*-planes of the crystallites parallel to graphene surface (Figure 4a), whereas some LDHs grow with *ab*-planes perpendicular to graphene surface (Figure 4b). And the LDHs with ab-planes perpendicular to graphene surface are easily formed in the compact LDHs growth region. TEM image (Figure 5a) of nanosized LDHs/GO hybrid indicates that two-dimensional GO has been decorated with many LDHs
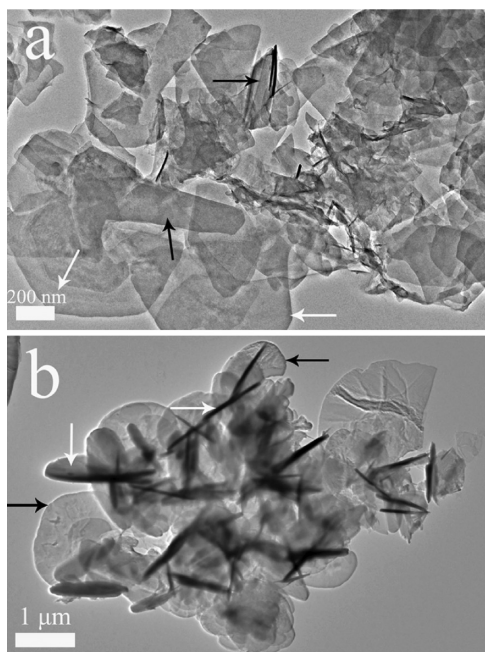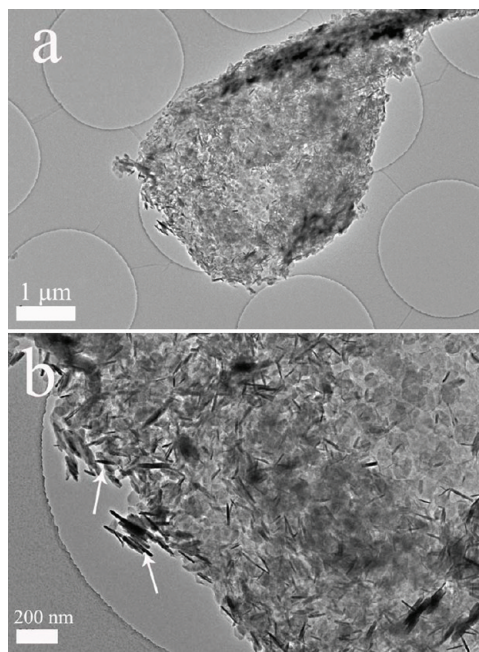
**Figure 4.** TEM images of microsized LDHs/GO hybrid.
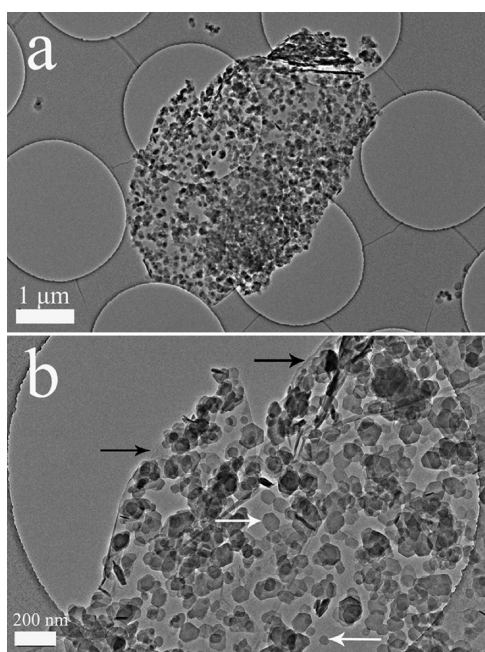


**Figure 5.** (a) Low- and (b) high-magnification TEM images of nanosized LDHs/GO hybrid at low LDHs nuclei concentration.



**Figure 6.** (a) Low and (b) high magnification TEM images of nanosized LDHs/GO hybrid at high LDHs nuclei concentration.

To thoroughly investigate the growth mechanism of LDHs on GO, GO film is fabricated and used as substrate to grow LDHs. Compared with individual GO nanosheets, GO film has much larger surface, and various kinds of LDHs can be grown on the same GO film substrate. Thus, it is much more convenient to observe the morphology of LDHs at a scale of tens of micrometers. As shown in Figure 7, GO film is
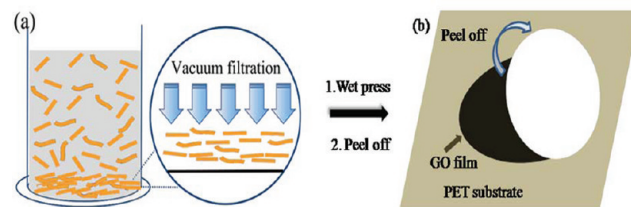


**Figure 7.** Schematic description of preparation of GO thin films and subsequent printing on a substrate.

nanoparticles before. At higher magnification (Figure 5b), it can be seen that the nanosized LDHs platelets are randomly laid on the GO nanosheets. The distribution of the decorating LDHs is not uniform because the GO sheets capture the LDHs mainly via reactive groups, and the active sites of GO are not homogeneously distributed on the nanosheets. LDHs deposited on the GO sheets still have hexagonal shape. If the ratio of LDHs nuclei to GO nanosheets significantly increases, LDHs grow much more densely on the surface of GO nanosheets (as shown in Figure 6a). At high magnification, LDHs with *ab*-planes of the crystallites perpendicular to GO nanosheets surface are observed, as indicated by white arrows in Figure 6b.

fabricated by vacuum-filtration induced self-assembly, followed by printing on PET film. In the presence of vacuum pressure, GO nanosheets were deposited on the membrane filter with preferential plane orientation. Due to strong affinity of GO nanosheets with water molecules, the filtrated GO thin film usually uptakes a small amount of water, which will act as ink solvent during the printing process. The wetted GO film on filter membrane was pressed against substrate surface. After holding an appropriate pressure for 20 min, the membrane filter was torn off, thus leaving an oriented, black, strong and flexible GO thin film adhering to the substrate. As a representative substrate, PET film is proved to be suitable to support GO film (with appropriate film thickness less than 10 $\mu$m) during the printing process, as shown in Figure S4a in the Supporting Information. Close inspection by SEM observation (Figure S4b) shows that the surface of GO film is rather flat. The as-prepared GO film was used as substrate and immersed in ion solution for in situ growth of Co−Al LDHs. At low ion

2245

dx.doi.org/10.1021/am300247x | ACS Appl. Mater. Interfaces 2012, 4, 2242−2249

concentration ($[\text{Co}^{2+}]$ = 5 mM, $[\text{Al}^{3+}]$ = 2.5 mM), the LDHs crystallites oriented with their *ab*-faces perpendicular and parallel to the substrate were observed simultaneously, as shown in Figure 8a. However, the LDHs crystallites oriented
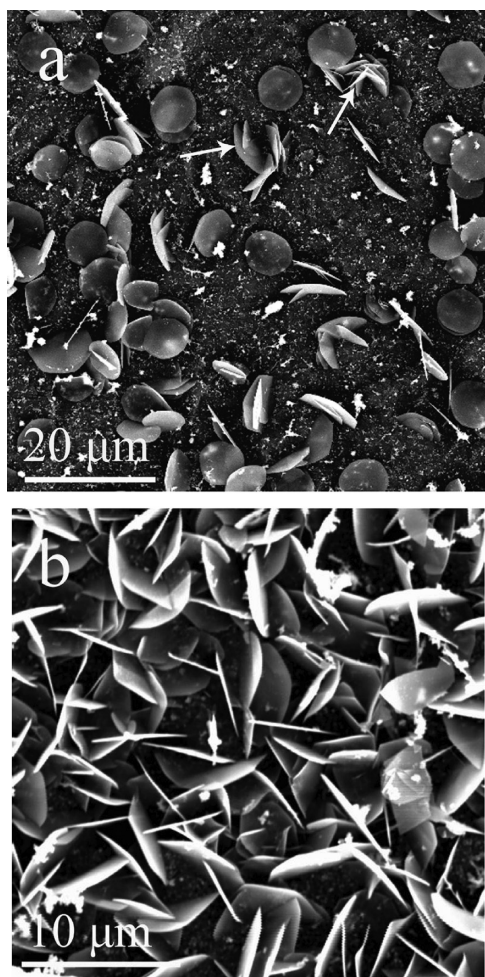


**Figure 8.** SEM images of in situ growth of Co−Al LDHs on GO film at (a) low and (b) high ion concentrations.

with their *ab*-faces perpendicular to the substrate are more easily formed in the dense LDHs growth region, as indicated by white arrows. At high ion concentration ($[\text{Co}^{2+}]$ = 20 mM, $[\text{Al}^{3+}]$ = 10 mM), only the LDHs with *ab*-planes perpendicular to graphene surface are observed, as shown in Figure 8b. Therefore, the preferred orientation of LDHs is related to their growth density on the GO film.

Preferential orientation during LDHs crystal growth on solid surfaces has been observed for a variety of substrate materials, including Aluminum and glass substrate.[11,25] Herein, "evolution selection" which has used to explain the preferred orientation of a vapor-deposited PbO layer is employed to explain the growth mechanism of LDHs on graphene oxide.[25,26] According to this mechanism, if the growth rates along different crystallographic axes are not same, the direction with the fastest growth rate makes a different angle to the normal to the surface for each crystal. When two crystals meet, the less steeply growing crystal is prevented from further growth by the more steeply growing crystal, which continues to grow. Repetition of this process ensures that crystals with the fastest growth direction normal to the substrate eventually envelop all the other crystals and finally

dominate the film. In case of the anisotropic LDHs crystallites, growth in the *ab*-direction is obviously faster than that in the *c*-direction. At low ion or nuclei concentrations, the density of LDHs on the surface is not high, both LDHs crystallites oriented with their *ab*-faces perpendicular and parallel to the GO film were observed, and LDHs with *ab*-faces perpendicular to substrate are easily formed in the dense nucleation area. At higher ion or nuclei concentrations, the nucleation density of LDHs on the whole GO film significantly increases. Thus, the growth of LDHs crystallites with their *ab*-planes perpendicular to the substrate becomes dominant on the GO film surface.

So far, various types of reduction methods have been reported to obtain GO sheets, such as the chemical reagent reduction, photochemical reduction, thermal reduction, and so on.[13] Among these methods, hydrothermal treatment is effective for the reduction of GO. Chemical analysis of powder samples of GO and LDHs/GO hybrid were conducted by XPS, and the C1s XPS spectra are shown in Figure 9. The C1s spectrum can be decomposed into four components: (1) the aromatic linked carbon (C=C, 284.8 eV), (2) the C in oxygen single-bonded carbon bonds (C−O, 286.2 eV), (3) the
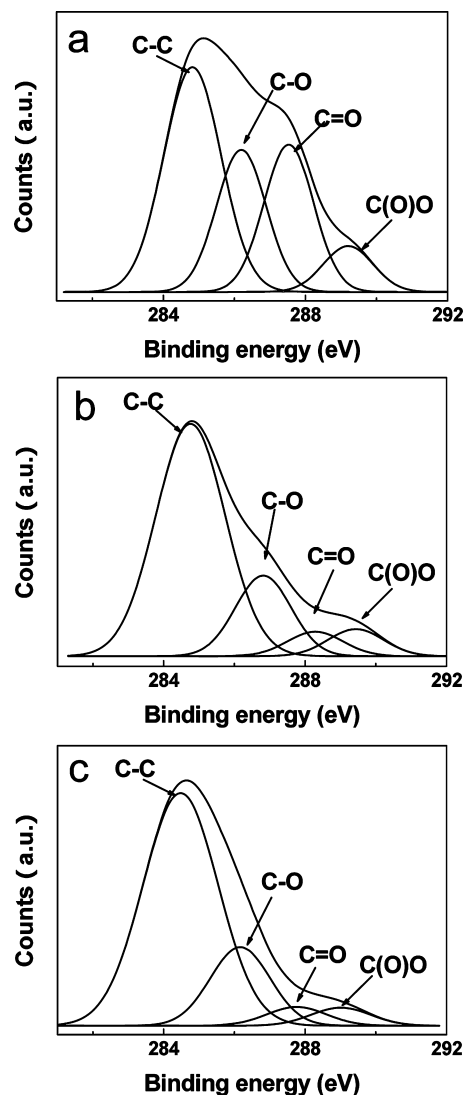


**Figure 9.** C1s XPS spectra of (a) GO, (b) microsized LDHs/GO hybrid, and (c) nanosized LDHs/GO hybrid.

carbonyl C (C=O, 287.8 eV), and (4) the carboxylate carbon (O−C=O, 289.0 eV).[27] In Figure 9a, GO shows a main peak at 284.6 eV, which corresponds to the component of C=C. Two strong peaks at 286.2 and 287.8 eV are also observed, suggesting considerable degree of oxidation in the graphite plane. For LDHs/GO hybrid sample (Figure 9b,c), the resolved spectrum of the C1s line shows two peaks at 284.8 and 287.8 eV, which are related to C=C and C=O bonds, respectively. Compared with GO, the signal of oxygen single-bonded carbon decrease and the oxygen double-bonded carbon becomes much weaker, confirming a successful reduction of GO. The significant structural changes are also reflected in the Raman spectra (see Figure S5 in the Supporting Information). For the graphene and GO, there are always two peaks appearing at about 1590 and 1335 cm$^{-1}$, known as G-band and D-band. The D-band is a combination of an $A_{1g}$ symmetry optical phonon at the $K$ point of the Brillouin zone because of the breathing vibration of aromatic rings, while the G-band corresponds to the first order scattering of $E_{2g}$ mode. As shown in Figure S5 in the Supporting Information, the Raman spectrum of GO shows a D-band to G-band intensity ratio ($I_D/I_G$) of 0.87. For the microsized LDHs/GO hybrid and nanosized LDHs/GO hybrid, the intensity ratio of D/G band increases to 1.22 and 1.27, respectively. This change suggests that new graphitic domains are created after hydrothermal treatment.[28]

The XRD patterns of graphite oxide and Co−Al LDHs/GO hybrid material are shown in Figure 10. Graphite oxide has a
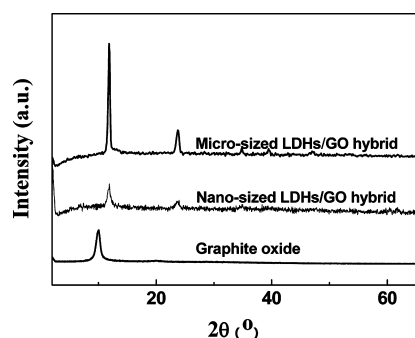


**Figure 10.** XRD curves of graphite oxide, microsized LDHs/GO hybrid, and nanosized LDHs/GO hybrid.

diffraction peak centered at $2\theta = 10.0°$, corresponding to (002) interplanar spacing of 8.8 Å, showing the oxidation of graphite into graphite oxide.[29] For LDHs/GO hybrid, the two diffraction peaks at $2\theta = 11.8$ and $23.7°$ correspond to (003) and (006) reflections of LDHs, and no characteristic (002) peaks of graphite oxide and graphite are observed. This suggests that the growth of LDHs can avoid the possibility of serious agglomeration and restacking of GO nanosheets during hydrothermal reduction.

**3.3. Electrochemical Performance of LDHs/GNS Hybrids.** To improve electrochemical performance, LDHs/GNS hybrid was prepared by reduction of LDHs/GO hybrid with hydrazine hydrate. Figure S6 in the Supporting Information shows the C1s XPS spectra of LDHs/GNS hybrid. Compared with LDHs/GO hybrid, the signal of oxygen single-bonded carbon decrease and the oxygen double-bonded carbon becomes much weaker, confirming a successful reduction from GO to GNS. To evaluate the electrochemical behaviors of the as-synthesized Co−Al LDHs and Co−Al LDHs/GNS hybrids for supercapacitor application, a series of CV and galvanostatic

charge/discharge measurements were carried out. Figure 11 shows the CV curves of the LDHs and LDHs/GNS hybrids at scan rates of 5, 10, 20, and 50 mV s$^{-1}$ in 1 M KOH solution. A couple of anodic/cathodic peaks are observed for CV curves of each sample at different scan rates, including the pure LDHs (Figure 11a, c) and LDHs/GNS hybrids (Figure 11b, d), indicating that faradic redox reactions of Co−Al LDHs are involved during the charge and discharge processes for contributing to the pseudocapacitance. According to the viewpoint of Scavetta et al.,[30,31] OH$^-$ ions replace the interlayer anions rapidly as soon as the electrode is dipped into KOH solution, thus the redox reaction can be written as

$$\text{LDH} - \text{Co(II)} + \text{OHsol}^-$$
$$\leftrightarrow \text{LDH(OH}^-) - \text{Co(III)} + e^- \qquad (1)$$
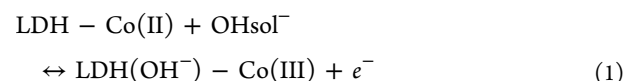
Besides, when the scan rate increases, the anodic and cathodic peaks move toward positive and negative direction, respectively. It is noteworthy that the LDHs/GNS hybrids show a smaller potential difference ($\Delta E_{a,c}$) between the anodic and cathodic peaks than pure LDHs under the same scan rate, demonstrating a better electrochemical reversibility of the LDHs/GNS hybrids. Moreover, the area surrounded by CV curves of the LDHs/GNS hybrids is obviously greater than that of pure LDHs, implying a higher electrochemical capacitance.

To evaluate the electrochemical capacitive property of pure LDHs and LDHs/GNS hybrid electrodes, we performed the galvanostatic charge/discharge measurements at various constant current densities of 0.5, 1, and 2 A g$^{-1}$. The specific capacitance of electrodes is calculated according to the following equation

$$Cs = \frac{I\Delta t}{m\Delta V} \qquad (2)$$

where $I$, $\Delta t$, $\Delta v$, and $m$ are the constant current (A), discharge time (s), total potential deviation (V), and mass of active materials (g), respectively.

Figure 12 shows the charge/discharge curves of LDHs and LDHs/GNS at current density of 2 A g$^{-1}$. It can be seen that specific capacitance of pure microsized LDHs and nanosized LDHs electrodes are 466.5 and 360.7 F/g, respectively. According to XRD results, the microsized LDHs show a higher crystallinity than nanosized LDHs, which may account for the higher discharge specific capacitances. Dai et al. also found the large-sized and high crystallinity Ni(OH)$_2$/graphene hybrid shows better electrochemical performance than the small-sized and low crystallinity Ni(OH)$_2$/graphene hybrid.[32]

Both the microsized LDHs/GNS and nanosized LDHs/GNS hybrids give a remarkably improved capacitance at different current rates, which are calculated by taking into account the ratio of LDHs in the hybrids (74 and 70% for microsized and nanosized LDHs/GNS hybrids, respectively, as determined by ICP). Specifically, at a high current of 2 A g$^{-1}$, the microsized LDHs and nanosized LDHs hybrids give a prominent discharge specific capacitance of 581.6 and 484.8 F/g, which are increased by 25% and 34% when compared with their pure LDHs counterparts. The prominent capacitive behavior is mainly attributed to the high electronic conductivity of the LDHs/GNS hybrids, which comes from two sources of intrinsic high conductivity of the GNS and interaction between the LDHs and the GNS in the hybrids. The anchored LDHs particles play an active role in preventing the aggregation of the graphene sheets, which connect with each other to further establish a

2247

dx.doi.org/10.1021/am300247x | ACS Appl. Mater. Interfaces 2012, 4, 2242−2249
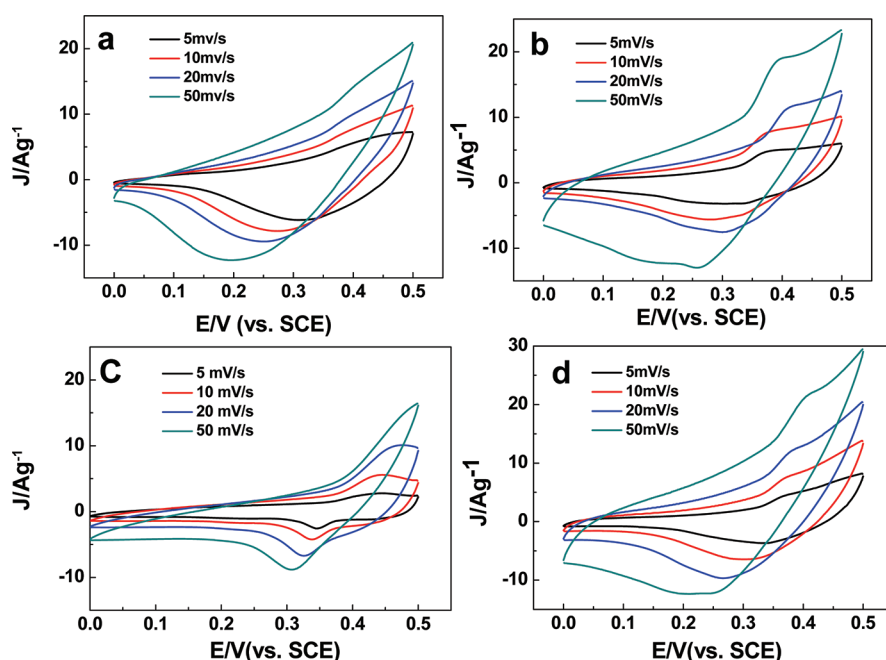
**Figure 11.** CV curves at different scan rates of (a) microsized LDHs, (b) microsized LDHs/GNS hybrid, (c) nanosized LDHs, and (d) nanosized LDHs/GNS hybrid.
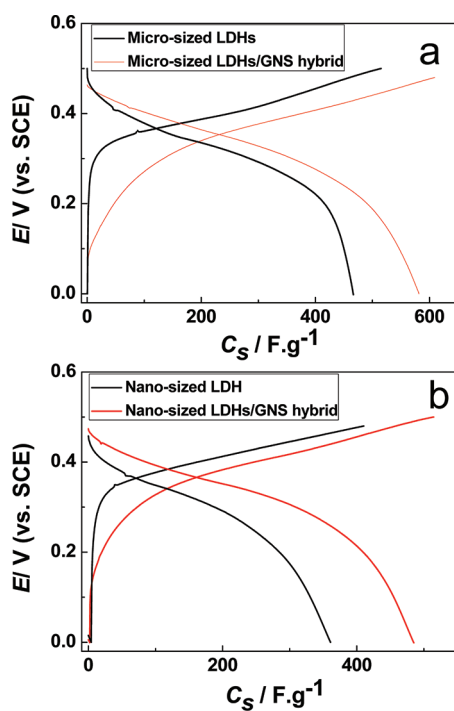


**Figure 12.** Charge/discharge curves at current density of 2 A g$^{-1}$ of (a) microsized LDHs and microsized LDHs/GNS hybrid, (b) nanosized LDHs and nanosized LDHs/GNS hybrid.

conductive network for facile electron transport. The high specific surface area of the LDHs/GNS hybrids favors the electrolyte percolation to achieve high accessibility of the LDHs active material, which also contributes to improved specific capacitance.[17,33]

## 4. CONCLUSIONS

Microsized and nanosize Co−Al−CO$_3$ LDHs were successfully grown on the surface of graphene oxide by hydrothermal method. GO nanosheets are simultaneously reduced into graphene due to the hydrothermal treatment. The formation of Co−Al LDHs platelets on the graphene nanosheets prevent the restacking of the as-reduced graphene nanosheets. LDHs/GO hybrid has complex structures, which depends on the concentrations of ion and LDHs nuclei. At low ion and LDHs nuclei concentrations, LDHs crystallites grow randomly with their *ab*-faces both perpendicular and parallel to the substrate. At higher ion or LDHs nuclei concentrations, LDHs are apt to grow with *ab*-planes perpendicular to GO nanosheets surface. "Evolution selection" growth mechanism was employed to explain this phenomenon. Furthermore, LDHs and LDHs/GNS hybrids were used as electrochemical supercapacitors materials and characterized by CV and galvanostatic charge/discharge measurements. The specific capacitances of LDHs are significantly enhanced by presence of GNS. Facile electron transport between individual nanoplatelets and the GNS may contribute to the improvement of specific capacitances of the LDHs.

## ■ ASSOCIATED CONTENT

### Ⓢ Supporting Information

FTIR spectra of LDHs samples (Figure S1), TEM image of GO sheets (Figure S2), AFM image and height profile of exfoliated GO sheets (Figure S3), photograph and SEM image of GO thin film printed on PET plastic film (Figure S4), Raman spectra of GO and LDHs/GO hybrids (Figure S5), C1s XPS spectra of LDHs/GNS hybrid (Figure S6). This material is available free of charge via the Internet at http://pubs.acs.org.

## ■ AUTHOR INFORMATION

**Corresponding Author**
*E-mail: txliu@fudan.edu.cn. Tel: +86-21-55664197. Fax: +86-21-65640293.

**Notes**
The authors declare no competing financial interest.

## ■ REFERENCES

(1) Mas, V.; Dieuzeide, M. L.; Jobbagy, M.; Baronetti, G.; Amadeo, N.; Laborde, M. *Catal. Today* **2008**, *133*, 319.

(2) Zhao, Y. F.; Wei, M.; Lu, J.; Wang, Z. L.; Duan, X. *ACS Nano* **2009**, *3*, 4009.

(3) Reinholdt, M. X.; Babu, P. K.; Kirkpatrick, R. J. *J. Phys. Chem. C* **2009**, *113*, 3378.

(4) Hussein, M. Z.; Zainal, Z.; Yahaya, A. H.; Foo, D. W. V. *J. Controlled Release* **2002**, *82*, 417.

(5) Yan, D. P.; Lu, J.; Wei, M.; Qin, S. H.; Chen, L.; Zhang, S. T.; Evans, D. G.; Duan, X. *Adv. Funct. Mater.* **2011**, *21*, 2497.

(6) Zhao, X. F.; Zhang, F. Z.; Xu, S. L.; Evans, D. G.; Duan, X. *Chem. Mater.* **2010**, *22*, 3933.

(7) Zhu, H.; Wang, W.; Liu, T. X. *J. Appl. Polym. Sci.* **2011**, *122*, 273.

(8) Peng, H. D.; Tjiu, W. C.; Shen, L.; Huang, S.; He, C. B.; Liu, T. X. *Compos. Sci. Technol.* **2009**, *69*, 991.

(9) Guo, X. X.; Zhang, F. Z.; Evans, D. G.; Duan, X. *Chem. Commun.* **2010**, *46*, 5197.

(10) Liu, J. P.; Li, Y. Y.; Huang, X. T.; Li, G. Y.; Li, Z. K. *Adv. Funct. Mater.* **2008**, *18*, 1448.

(11) Guo, X. X.; Zhang, F. Z.; Xu, S. L.; Evans, D. G.; Duan, X. *Chem. Commun.* **2009**, *44*, 6836.

(12) Hsieh, Z. L.; Lin, M. C.; Uan, J. Y. *J. Mater. Chem.* **2011**, *21*, 1880.

(13) Huang, X.; Qi, X. Y.; Boey, F.; Zhang, H. *Chem. Soc. Rev.* **2012**, *41*, 666.

(14) Zhu, Y. W.; Murali, S.; Cai, W. W.; Li, X. S.; Suk, J. W.; Potts, J. R.; Ruoff, R. S. *Adv. Mater.* **2010**, *22*, 3906.

(15) Liu, X. M.; Zhang, Y. H.; Zhang, X. G.; Fu, S. Y. *Electrochim. Acta* **2004**, *49*, 3137.

(16) Li, H. J.; Zhu, G.; Liu, Z. H.; Yang, Z. P.; Wang, Z. L. *Carbon* **2010**, *48*, 4391.

(17) Gao, Z.; Wang, J.; Li, Z. S.; Yang, W. L.; Wang, B.; Hou, M. J.; He, Y.; Liu, Q.; Mann, T.; Yang, P. P.; Zhang, M. L.; Liu, L. H. *Chem. Mater.* **2011**, *23*, 3509.

(18) Huang, S.; Cen, X.; Peng, H. D.; Guo, S. Z.; Wang, W. Z.; Liu, T. X. *J. Phys. Chem. B* **2009**, *113*, 15225.

(19) Xu, Z. P.; Stevenson, G. S.; Lu, C. Q.; Lu, G. Q.; Bartlett, P. F.; Gray, P. P. *J. Am. Chem. Soc.* **2006**, *128*, 36.

(20) Xu, Z. P.; Stevenson, G.; Lu, C. Q.; Lu, G. Q. *J. Phys. Chem. B* **2006**, *110*, 16923.

(21) Hummers, W. S.; Offeman, R. E. *J. Am. Chem. Soc.* **1958**, *80*, 1339.

(22) Liu, Z. P.; Ma, R. Z.; Osada, M.; Iyi, N.; Ebina, Y.; Takada, K.; Sasaki, T. *J. Am. Chem. Soc.* **2006**, *128*, 4872.

(23) Evans, D. G.; Duan, X. *Chem. Commun.* **2006**, *5*, 485.

(24) Park, S.; Ruoff, R. S. *Nat. Nanotechnol.* **2009**, *4*, 217.

(25) Guo, X. X.; Xu, S. L.; Zhao, L. L.; Lu, W.; Zhang, F. Z.; Evans, D. G.; Duan, X. *Langmuir* **2009**, *25*, 9894.

(26) van der Drift, A. *Philips Res. Rep.* **1967**, *22*, 267.

(27) Yang, D.; Velamakanni, A.; Bozoklu, G.; Park, S.; Stoller, M.; Piner, R. D.; Stankovich, S.; Jung, I.; Field, D. A.; Ventrice, C. A.; Ruoff, R. S. *Carbon* **2009**, *47*, 145.

(28) Stankovich, S.; Dikin, D. A.; Piner, R. D.; Kohlhaas, K. A.; Kleinhammes, A.; Jia, Y.; Wu, Y.; Nguyen, S. T.; Ruoff, R. S. *Carbon* **2007**, *45*, 1558.

(29) Yang, Y.; Ren, L. L.; Zhang, C.; Huang, S.; Liu, T. X. *ACS Appl. Mater. Interfaces* **2011**, *3*, 2779.

(30) Su, L. H.; Zhang, X. G.; Liu, Y. *J. Solid State Electrochem.* **2008**, *12*, 1129.

(31) Scavetta, E.; Berrettoni, M.; Nobili, F.; Tonelli, D. *Electrochim. Acta* **2005**, *50*, 3305.

(32) Wang, H. L.; Casalongue, H. S.; Liang, Y. Y.; Dai, H. J. *J. Am. Chem. Soc.* **2010**, *132*, 7472.

(33) Wang, L.; Wang, D.; Dong, X. Y.; Zhang, Z. J.; Pei, X. F.; Chen, X. J.; Chen, B.; Jin, J. *Chem. Commun.* **2011**, *47*, 3556.